Journal of The Electrochemical Society, **153** (10) A1795-A1799 (2006)
0013-4651/2006/153(10)/A1795/5/$20.00 © The Electrochemical Society

Enhanced Pulse Power Polymer Electrolyte Membrane Fuel Cell Using Internal Hybrid Catalyst Layer Electrodes

Steven R. D'Souza,* Jianmxin Ma, and Chunsheng Wang,z**

Department of Chemical Engineering and Center for Manufacturing Research, Tennessee Technological University, Cookeville, Tennessee 38505

Novel internal polymer electrolyte membrane fuel cell/energy storage hybrid power systems were fabricated to improve the pulse power output of the system by incorporating a supercapacitor element ($Ru_2O{\cdot}0.5H_2O$) and a battery element ($CeZrO_2$) into the cathode catalyst layer of fuel cells. The steady-state performance of the hybrid fuel cell system was similar to that of the conventional fuel cell. However, the peak power output of the hybrid system, which was demonstrated by a potential square-wave voltammetry program, showed a much higher value than that of the conventional fuel cell. The pulse power output of the fuel cells can be enhanced markedly by incorporating a supercapacitor element or a battery element into the electrocatalyst layer.
 [DOI: 10.1149/1.2221777]

Manuscript submitted January 5, 2006; revised manuscript received April 6, 2006. Available electronically July 26, 2006. This was Paper 190 presented at the Los Angeles, CA, Meeting of the Society, Oct 16–21, 2005.

Polymer electrolyte membrane fuel cells (PEMFCs) generate power for stationary/portable devices and show promise for automobile applications. They are advantageous over traditional power generators due to their light weight, high power density, and low generation of emissions.[1] However, their ratio of peak to continuous power and response to instantaneous loads is often insufficient. In addition, meeting peak power demands for vehicular applications such as starting, accelerating, and uphill driving is difficult. To meet such peaking power demands, the PEMFC must be hybridized with a supercapacitor or a high-power secondary battery.[2]

Normally, hybrid fuel cell/battery or supercapacitor systems use separate components which are connected by electrical control subsystems. This results in increased complexity, weight, volume, and cost.[2,3] To overcome these drawbacks of the conventional hybrid power system, we proposed a novel concept of the internal fuel cell/battery or supercapacitor system.[4,5] In this way, a battery element and/or a supercapacitor element was incorporated into the fuel cell system. So far, we have successfully inserted a supercapacitor element sublayer directly into a PEM fuel cell[4] and an alkaline fuel cell.[5] The previous results showed that the peak power of the internal PEMFC/supercapacitor ($RuO_2{\cdot}xH_2O$) system was two times higher than that of the conventional fuel cell system, but the continual power of the hybrid system was slightly inferior to that of the conventional system due to additional proton transportation resistance of the supercapacitor sublayer. It is expected that the continual power output of the internal fuel cell/supercapacitor (or battery) system will be improved without sacrificing peak power output if the supercapacitor (or battery) element is incorporated into the catalytic layer of the fuel cell to form a composite active layer. Moreover, if the inserted energy storage element has a high energy storage capacity and good catalytic activity for hydrogen oxidation and oxygen reduction, the internal fuel cell/energy storage hybrid power sources may have much higher power and energy than that of conventional fuel cells.

Cerium oxide (CeO_2), an oxygen storage material, can be considered as a battery element. The excellent ability of CeO_2 to store oxygen is a result of the delicate balance between the structural (atomic and phase composition), kinetic (ability to shift easily between the reduced and oxidized states: Ce^{3+} Ce^{4+}), and textural (presence of surface cerium factors) properties.[6] Ceria (Ce) equilibrium with oxygen pressure is shown by:

$$CeO_2 \rightleftharpoons CeO_{2-x} + \left(\frac{x}{2}\right)O_2 \quad (0 \le x \le 0.5) \qquad [1]$$

CeO_2 is doped with zirconia oxide (ZrO_2) forming a $CeZrO_2$ solid solution, thereby increasing the thermal stability and oxygen storage capacity of the material. The insertion of ZrO_2 into the CeO_2 lattice distorts the oxygen sublattice, making mobile oxygen available for redox processes.[7] Several papers have been published to study the effect of oxygen storage materials such as CeO_2 and $Ce_{0.8}Zr_{0.2}O_2$ incorporated into the cathode on the performance of fuel cells.[8,9] The steady-state performance of the Pt-$Ce_{0.8}Zr_{0.2}O_2$ fuel cell was almost the same as or slightly less than the Pt fuel cell.[8] The $Ce_{0.8}Zr_{0.2}O_2$ oxygen storage material in the cathode side of the fuel cell can be considered a rechargeable battery element. It absorbs and stores oxygen (at the fully charged state) when the fuel cell operates at a high voltage and high oxygen partial pressure. However, it desorbs oxygen (battery discharging) when the fuel cell suddenly jumps to a low voltage with a low local oxygen pressure at the cathode. The amount of released oxygen from storage materials decreases with time and gradually equilibrates with low oxygen pressure. Therefore, the oxygen storage material incorporated into the fuel cell delivers/absorbs additional energy only under instantaneous power load conditions and has no influence on the continual power output of the fuel cell. This is the reason why incorporating CeO_2 and $Ce_{0.8}Zr_{0.2}O_2$ (or V_2O_5) oxygen storage materials into the cathode of the fuel cell did not improve the continual power output of the fuel cell.[8,9] The effects of energy storage elements in a fuel cell should only be evaluated using the transient-state measuring method rather than the steady-state method.

In this paper, we prepared an internal PEMFC/supercapacitor hybrid system and an internal PEMFC/battery hybrid system by incorporating $RuO_2{\cdot}0.5H_2O$ (supercapacitor element) and $Ce_{0.86}Zr_{0.14}O_2$ (rechargeable battery element), respectively, into the cathode catalyst layer of the PEMFC. The performance of these hybrid systems was evaluated under the transient-state and the steady-state conditions.

Experimental

Preparation of gas diffusion electrodes and membrane-electrode-assemblies.— A thin gas diffusion layer (GDL) was prepared by spreading Shawinigan acetylene black (Chevron-Texaco, Houston, TX) containing 35 wt % polytetrafluoroethylene (PTFE) on Textron CPW-003 lightweight carbon cloth (Wilmington, MA). Three different cathodes were fabricated by painting the inks mixed with different electrocatalysts with 5% Nafion solution (DuPont) in the mass ratio of 3:1 onto the GDL. These three electrocatalysts were: (*i*) pure 40 wt % Pt/C catalyst (E-TEK), (*ii*) a mixture of 40 wt % Pt/C and $RuO_2{\cdot}xH_2O$ with the mass ratio of 1:0.73, and (*iii*) a mixture of 40 wt % Pt/C and $Ce_{0.86}Zr_{0.14}O_2$ (Alfa Aesar) with the mass ratio of 1:1, respectively. RuO_2 with different amounts of bound water ($RuO_2{\cdot}xH_2O$) was obtained by annealing hydrous ruthenium oxide $RuO_2{\cdot}1.9H_2O$ (Alfa Aesar) in air at 150, 200, and

* Electrochemical Society Student Member.
** Electrochemical Society Active Member.
z E-mail: cswang@tntech.edu

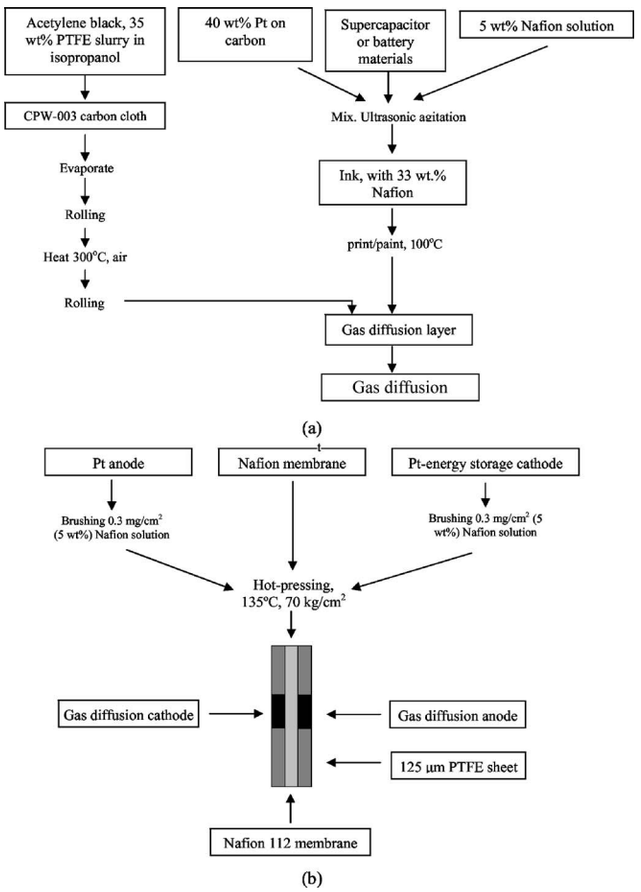

Figure 1. Preparation of (a) gas diffusion electrode and (b) MEA used for the internal PEMFC/energy storage hybrid power system.

240°C for 2 h to eliminate water and increase crystallinity. The mixture was agitated in an ultrasonic bath for 2 h and stirred thoroughly before applying to the GDL. The anode was prepared in the same way as the cathode but used 40 wt % Pt/C catalyst with Pt loading of 0.2 mg/cm^2.

Membrane electrode assemblies (MEAs) were prepared by hot pressing Pt/C, Pt/C–$RuO_2{\cdot}xH_2O$, or Pt/C–$CeZrO_2$ cathodes and Pt anodes, which were then placed symmetrically on both sides of a Nafion 112 membrane and pressed with 70 kg/cm^2 of pressure for 4 min at 135°C. Before pressing the MEAs, the surfaces of the GDE were impregnated with ca. 0.3 mg/cm^2 Nafion by brushing with a 5 wt % solution. The geometric area of all MEAs was 1.0 cm^2. To increase the effective surface area of the cathode, two cathodes with Nafion loading of 16 and 33 wt % were used. The composite electrode with 16 wt % Nafion loading was prepared by adding $RuO_2{\cdot}0.5H_2O$ (or $CeZrO_2$) into Pt/C-33% Nafion ink, and the 33 wt % Nafion electrode was prepared by mixing $RuO_2{\cdot}0.5H_2O$-33% Nafion (or $CeZrO_2$-33% Nafion) into Pt/C-33% Nafion ink. The electrochemical active surface area of the two MEAs was compared using cyclic voltammetry (CV), which was measured in the potential range of 0.1–1.0 V at the cell operating temperature of 50°C with N_2 flowing at the cathode side and humidified H_2 into the anode side. The columbic charge under the hydrogen adsorption and desorption peaks of the cathode with 33 wt % Nafion loading is larger than the electrode with 16 wt % Nafion loading. Therefore, 33 wt % Nafion loading was used to prepare the composite cathodes. A flow chart for GDL and MEA preparation is shown in Fig. 1.

The schematic illustration of the hybrid fuel cell system under

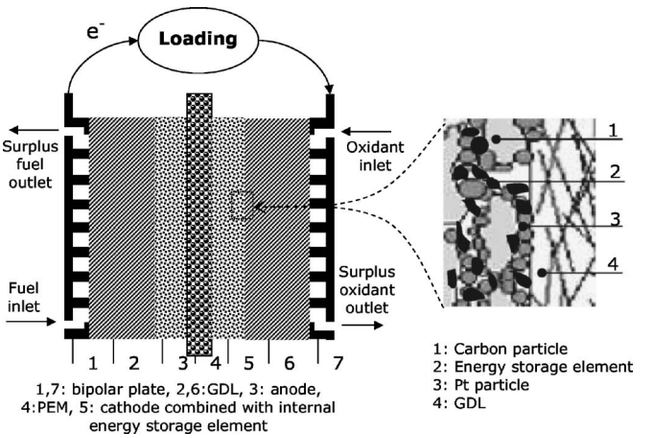

Figure 2. Schematic illustration of the internal PEMFC/energy storage hybrid power system.

investigation is shown in Fig. 2. Unlike the structure of the multilayer electrode MEAs fabricated in our previous design,[4] where $RuO_2{\cdot}xH_2O$ was inserted between the membrane and the catalyst layer to form a supercapacitor sublayer, the supercapacitive element ($RuO_2{\cdot}xH_2O$) or battery element ($CeZrO_2$) were directly incorporated into the catalyst layer to form an integrated composite layer.

Capacitance measurement of the supercapacitor and oxygen storage materials.— The capacitance (energy storage capacity) of the fuel cells with the Pt/C-$RuO_2{\cdot}xH_2O$ supercapacitor and the Pt/C-$CeZrO_2$ oxygen storage was evaluated using CV between −0.5 and +0.5 V at scan rates of 1, 5, 10, and 20 mV/s, respectively. The CV of the samples was measured using a Solartron model 1287 electrochemical interface at a cell operating temperature of 50°C with pure nitrogen humidified at 50°C at both the anode and cathode sides. The peak current density outputs for the fuel cells under the same operating conditions were measured using the potential square-wave voltammetry with the programs shown in Fig. 3.

Performance measurement of the fuel cells.— MEA disks with a geometric area of 1.0 cm^2 were tested in a single cell with a serpentine flow channel. The cell was operated at 50°C and the hydrogen and oxygen were prehumidified with sparing bottles at a temperature of 50°C. Before polarization measurement, the cell was activated by

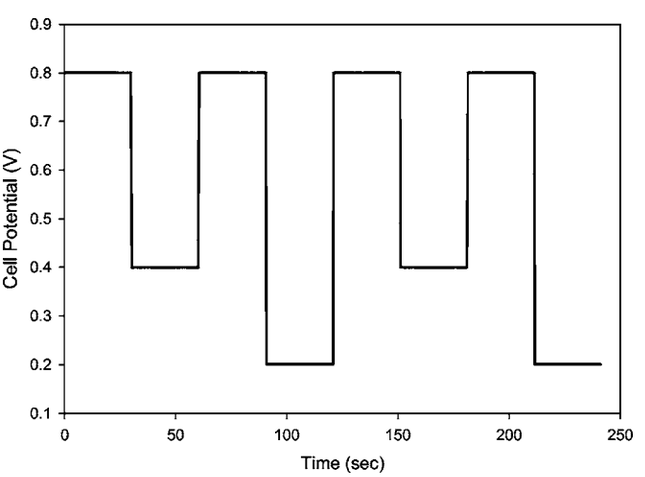

Figure 3. Potential square-wave voltammetry program used to evaluate the peak power the internal PEMFC/energy storage hybrid power system.

Table I. The composition of $RuO_2 \cdot 1.9H_2O$ after annealing at 150, 200, and 250°C for 2 h.

Sample no.	1	2	3
Temperature (°C)	240	200	150
Initial mass (g)	1.0014	1.001	1.001
Final mass (g)	0.8182	0.8343	0.8555
Weight loss (%)	18.29	16.65	14.54
Final composition	$RuO_2 \cdot 0.19H_2O$	$RuO_2 \cdot 0.34H_2O$	$RuO_2 \cdot 0.54H_2O$

repeating operation with a rest at open-circuit potential (OCP) for 1 h, followed by conditioning at 0.4 V for a 30 min and 0.2 V for another 30 min until a steady current was achieved. The continual power outputs of the fuel cells with Pt/C only, Pt/C-$RuO_2 \cdot xH_2O$, and Pt/C–$CeZrO_2$ were obtained by potential-scanning from the OCP to zero at the scan rate of 1 mV/s using a Solartron model 1287 electrochemical interface. In order to verify reproducibility and reliability of the steady-state results, the polarization curves obtained by potential-scanning were also compared with the data measured using a HP data acquisition system. These results were almost the same.

The peak power of the integrated hybrid fuel cell system contributed from the supercapacitor element ($RuO_2 \cdot 0.5H_2O$) as well as that of the battery element ($CeZrO_2$) was measured under pulsed voltage conditions using the potential square-wave voltammetry program as shown in Fig. 3. In the potential square-wave voltammetry program, a potential of 0.8 V was applied for a specified period of time, stepped to a different value, and then the corresponding current peak was measured.

Results and Discussion

Capacitance characteristics of annealed $RuO_2 \cdot 1.9H_2O$.— It was found that the electronic conductivity of hydrous ruthenium oxide increases with increasing crystallinity; however, proton diffusion decreases.[10] Therefore, the maximum utilization of the energy storage ability of $RuO_2 \cdot xH_2O$ can be achieved when both electron and proton transport are at an optimum value. After annealing at the three different temperatures (150, 200, and 240°C), $RuO_2 \cdot 1.9H_2O$ had various weight losses and thereby the corresponding formula of the composite was calculated and is shown in Table I. Decomposition of RuO_2 to Ru metal does not occur at temperatures less than 1000°C,[11] thus the weight loss can be attributed to the loss of bound water. The composition of $RuO_2 \cdot xH_2O$ after high temperature annealing treatment should be stable during fuel cell operation and capacitance measurement at 50°C because the adsorption of water on a RuO_2 (110) surface occurs between 77 and 152°C.[12] The capacitance (energy storage capacity) of annealed hydrous ruthenium oxide composites were measured using CV at a scan rate of 10 mV/s, as shown in Fig. 4, in a N_2 environment. As expected, the sample annealed at 150°C (solid black line) showed the highest capacitance equal to 400 F/g. This value is higher than 230 F/g reported by Wang et al.[4] but much lower than that of sol-gel $RuO_2 \cdot 0.5H_2O$, in sulfuric acid electrolyte (720 F/g).[13] A possible explanation for this is the smaller effective contact area between the larger RuO_2 particles and the solid polymer electrolyte. As expected, the capacitance decreased to 200 F/g when the heat-treatment temperature increased to 240°C. Therefore, the $RuO_2 \cdot 0.5H_2O$ prepared by annealing $RuO_2 \cdot 1.9H_2O$ at 150°C for 2 h was used for supercapacitor element in this work.

Capacitance characteristics of PEMFC with and without $RuO_2 \cdot 0.5H_2O$ and $CeZrO_2$ addition.— To investigate the influence of the supercapacitor element ($RuO_2 \cdot 0.5H_2O$) and the battery element ($CeZrO_2$) on the capacitive performance of the PEMFCs, the capacitive behavior of the PEMFCs composed of the Pt/C–$RuO_2 \cdot 0.5H_2O$ electrode and the Pt/C–$CeZrO_2$ electrode, respectively, were measured by CV scanning under nitrogen atmosphere at 50°C. For comparison, the capacitive behavior of the PEMFC composed of a Pt/C electrode was also tested under the same conditions. All CV curves exhibited ideal pseudocapacitive behavior between −0.5 and +0.5 V. The charge and discharge currents increased linearly with scan rate, as expected. Figure 5 shows the CV curves of the PEMFCs with and without energy storage addition under the scan rate of 5 mV/s. Among these three fuel cells, the Pt/C-$RuO_2 \cdot 0.5H_2O$ device exhibited the highest capacitance, followed by the Pt/C–$CeZrO_2$ device, and the Pt/C device exhibited the worst capacitance behavior. The specific capacitance of the Pt/C–$RuO_2 \cdot 0.5H_2O$ device is calculated to be 400 F/g, and the values of the Pt/C–$CeZrO_2$ device and the Pt/C device are 100 and 50 F/g, respectively. The superior capacitive performance of the Pt/C–$RuO_2 \cdot 0.5H_2O$ device can be contributed to the perfect pseudocapacitive characteristic of RuO_2 material. The low capacitance characteristics of the Pt/C device is related to the carbon black (used for electrocatalyst support), which is a conventional material used for double-layer capacitors. It is well known that supercapacitors have a high specific power density, rapid charging/discharge

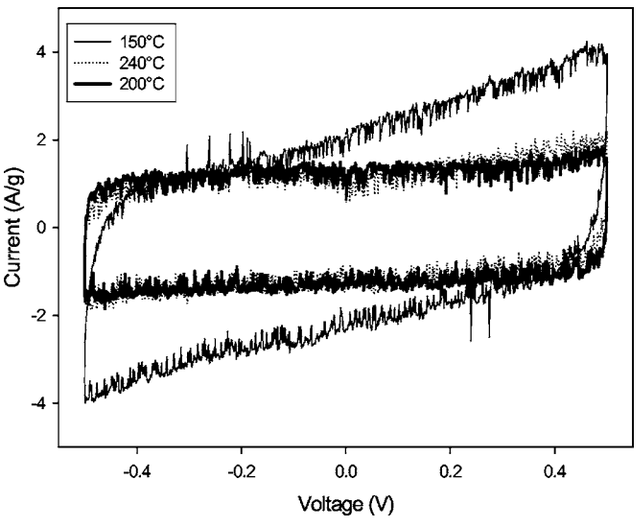

Figure 4. CV of the PEMFC with annealed $RuO_2 \cdot xH_2O$ addition at 10 mV/s in N_2 environment. Pt loading: 0.6 mg/cm^2, $RuO_2 \cdot xH_2O$ loading: 1.1 mg/cm^2.

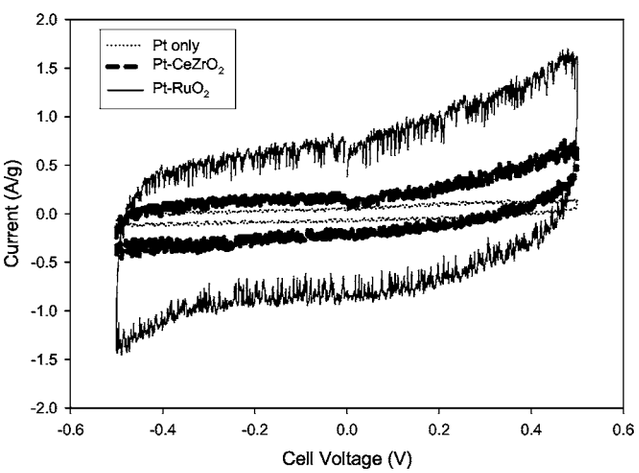

Figure 5. CV of the PEMFCs with and without energy storage element addition in N_2 environment at a scan rate of 5 mV/s. Pt loading: 0.3 mg/cm^2, CeZr loading: 0.6 mg/cm^2, $RuO_2 \cdot xH_2O$ loading: 0.6 mg/cm^2.

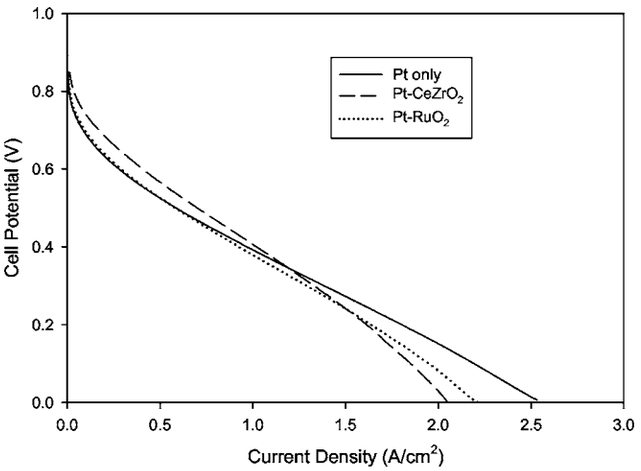

Figure 6. Steady-state performance of the PEMFCs with and without energy storage element addition. Pt loading: 0.3 mg/cm^2, $RuO_2 \cdot 0.5H_2O$ loading: 0.6 mg/cm^2; $CeZrO_2$ loading: 0.6 mg/cm^2.

behavior, and are capable of many cycles without perceptible capacity decay.[14] The Pt/C–$RuO_2 \cdot 0.5H_2O$ device is therefore expected to have a high peak power output due to the high capacitive performance.

Steady-state performance of PEMFCs with and without $RuO_2 \cdot 0.5H_2O$ and $CeZrO_2$ addition.— Figure 6 shows the steady-state performance of the PEMFCs with and without energy storage elements addition. The open-circuit voltage of the fuel cells with and without energy storage addition were the same, which indicates that $RuO_2 \cdot 0.5H_2O$ and $CeZrO_2$ addition into the catalyst layer did not influence the equilibrium potential of oxygen reduction. In Fig. 6, the incorporation of $CeZrO_2$ into the catalyst layer slightly increased the steady-state performance of the PEMFC at low currents but decreased the performance at high currents. The slight influence of $CeZrO_2$ on the steady-state performance of the fuel cell is in agreement with reported results.[8,9] $RuO_2 \cdot 0.5H_2O$, in addition, has no influence on the low-loading performance but slightly decreased the steady-state power output at high-loading conditions. Our previous results showed that the insertion of a $RuO_2 \cdot 0.5H_2O$ sublayer between the membrane and the catalytic layer largely decreased the steady-state performance of the fuel cell at all loading regions.[4] Therefore, integrating an energy storage sublayer into the catalyst layer to form a single composite layer benefited the continual power output of PEMFCs.

Peak-power performance of PEMFC with and without $RuO_2 \cdot 0.5H_2O$ and $CeZrO_2$ addition.— Figure 7 shows the pulse-loading performance of the PEMFCs with and without $RuO_2 \cdot 0.5H_2O$ and $CeZrO_2$ addition under the humidified nitrogen atmosphere. For the PEMFC without an energy storage element, the pulse current output was only approximately 3 A/g, which was attributed to the double-layer capacitance of carbon black used for supporting the platinum electrocatalyst. Incorporating $CeZrO_2$ into the catalyst layer gave the PEMFC double the peaking current with about 7 A/g. Mixing $RuO_2 \cdot 0.5H_2O$ into the platinum electrocatalyst layer increased the peak current by seven times over $CeZrO_2$ to an average of 50 A/g. Thus, the rapid reaction kinetics and pseudocapacitor behavior of $RuO_2 \cdot 0.5H_2O$ greatly improved the peak current output of the PEMFC. Comparing the peak current in Fig. 7 with the capacity in Fig. 5, the peak-power performance of the PEMFCs with different energy storage additions was consistent with the corresponding capacitive behavior of the devices.

Figure 8 shows the square-wave load performance of the PEMFCs with and without $RuO_2 \cdot 0.5H_2O$ and $CeZrO_2$ addition at a constant baseline voltage of 0.8 V. It can be found that the peak current

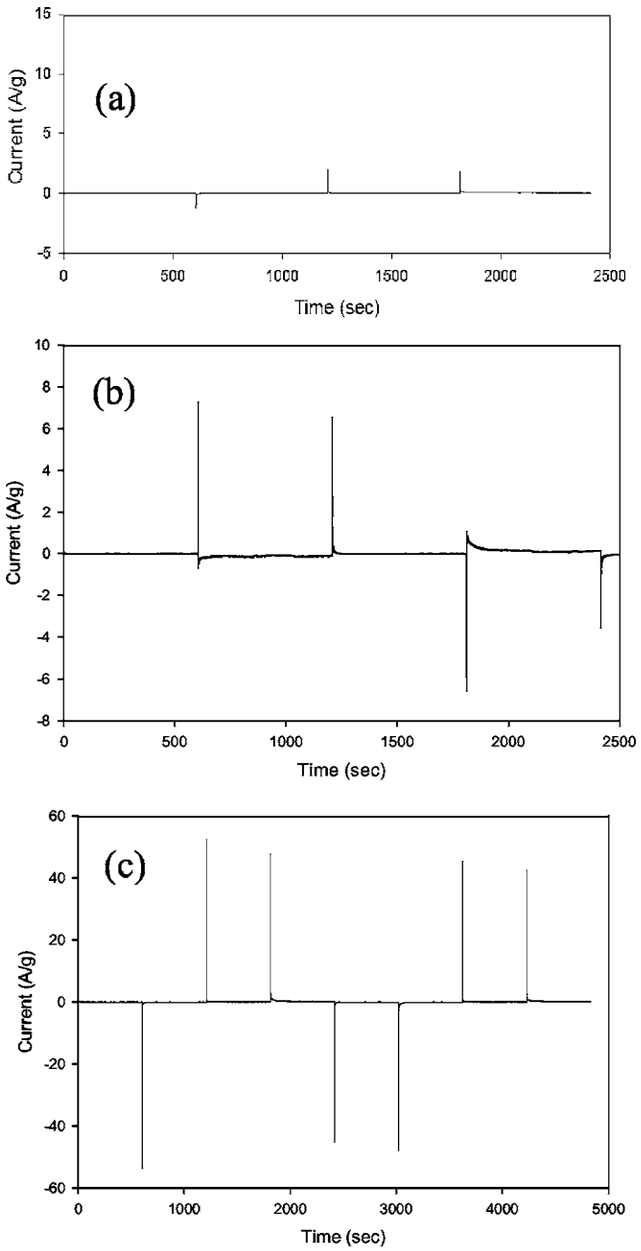

Figure 7. Pulse-loading performance of the PEMFCs with and without energy storage element addition measured using the pulse voltammetry program in Fig. 3 under the humidified nitrogen atmosphere, (a) Pt loading: 0.3 mg/cm^2, (b) Pt (0.3 mg/cm^2)-$CeZrO_2$ (0.6 mg/cm^2), and (c) Pt (0.3 mg/cm^2)-$RuO_2 \cdot 0.5H_2O$ (0.6 mg/cm^2).

of the PEMFCs increased by adding $RuO_2 \cdot 0.5H_2O$ and the $CeZrO_2$ into the catalyst layer, although the current at the end of voltage jump of the PEMFC without energy storage at a low voltage (0.2 V) is slightly higher than that of the fuel cells with $RuO_2 \cdot 0.5H_2O$ and $CeZrO_2$ addition. The current of the fuel cells with and without energy storage at the end of each jumping voltage in Fig. 8 is in agreement with the steady-state performance of the fuel cells in Fig. 6. Furthermore, the same peak current of the PEMFCs was observed when the operating voltage of the fuel cell jumped from the 0.8 V to the lower value (0.4 or 0.2 V) periodically. The phenomena indicated that the discharged supercapacitor/battery element at the lower voltage can be quickly recharged when the operating voltage of the

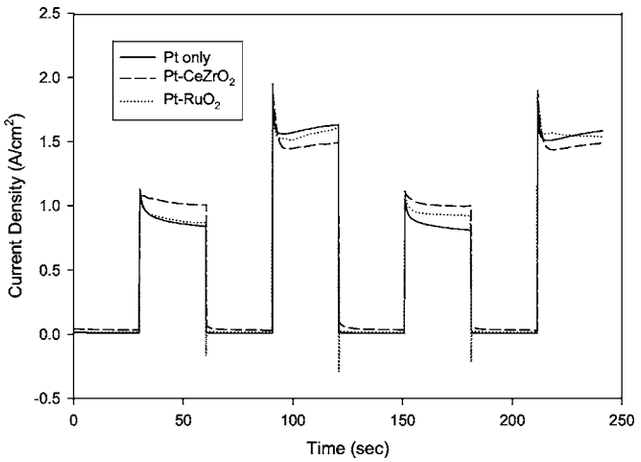

Figure 8. Pulse-loading performance of the PEMFCs with energy storage elements addition measured by the potential square-wave voltammetry program in Fig. 3. Pt loading: 0.3 mg/cm^2, $CeZrO_2$ loading: 0.6 mg/cm^2, $RuO_2 \cdot 0.5H_2O$ loading: 0.6 mg/cm^2.

fuel cell jumped back to 0.8 V. Therefore, the discharged supercapacitor/battery element can be recharged effectively during normal fuel cell operation.

The durability of PEMFC/energy storage hybrid power sources was tested by operating the fuel cell at 0.4 V for 1 week. The pulse loading performance of the fuel cell was checked daily. No obvious pulse response decay was found, which indicated that $RuO_2 \cdot 0.5H_2O$ and $CeZrO_2$ are stable during fuel cell operation.

Conclusions

The maximum capacitance (400 F/g) of $RuO_2 \cdot 0.5H_2O$ was achieved by annealing $RuO_2 \cdot 1.9H_2O$ in air at 150°C for 2 h. The high capacitance of $RuO_2 \cdot 0.5H_2O$ is due to the balanced electron and proton conductivities of $RuO_2 \cdot 0.5H_2O$.

Some novel internal PEM fuel cell/energy storage hybrid power systems were fabricated successfully by incorporating a supercapacitor element ($Ru_2O \cdot xH_2O$) or a battery element ($CeZrO_2$) into the catalyst layer of the cathode. The steady-state performance of the hybrid fuel cell system was similar to that of the conventional system, which was in agreement with the previous results reported by others. However, the peak power output of the intrinsic hybrid system is much higher than that of the conventional system. The excellent response to instantaneous loads of internal PEMFC/energy storage hybrid power systems was due to the high power of energy storage elements which were incorporated into the catalyst layer. The discharged supercapacitor and battery materials can be recharged during normal fuel cell operation. This modified PEM fuel cell performed the same functions as those of a more complex fuel cell/supercapacitor and fuel cell/battery hybrid system without significant increase in weight, volume, and cost. This power source can be used for a digital communication device application where the pulse output requirement is in the millisecond range.

Acknowledgments

This work was performed under the auspices of the Faculty Research Grant, Tennessee Technological University. The authors also appreciated a reviewer's comments and suggestions, which greatly improved the quality of this paper.

Tennessee Technology University assisted in meeting the publication costs of this article.

References

1. J. H. Hirschenhofer, D. B. Stauffer, and R. R. Engleman, in *Fuel Cell Handbook*, U. S. Department of Energy, Morgantown, WV (1994).
2. L. P. Jarvis, T. B. Atwater, and E. J. Plichta, *J. Power Sources*, **70**, 253 (1998).
3. A. Jossen, J. Garche, H. Doering, M. Goetz, W. Knaupp, and L. Joerissen, *J. Power Sources*, **144**, 395 (2005).
4. C. Wang and A. J. Appleby, *J. Electrochem. Soc.*, **150**, A493 (2003).
5. C. Wang, A. J Appleby, and D. L. Cocke, *J. Electrochem. Soc.*, **151**, A260 (2004).
6. A. Trovarelli, M. Boaro, E. Rocchini, C. D. Leitenburg, and G. Dolcetti, *J. Alloys Compd.*, **323-324**, 584 (2001).
7. G. Vlaic, P. Fornasiero, S. Geremia, J. Kaspar, and M. Graziani, *J. Catal.*, **168**, 386 (1997)
8. Z. Xu, Z. Qi, and A. Kaufman, *J. Power Sources*, **115**, 40 (2003).
9. H. B. Yu, J. Kim, H. Lee, M. A. Scibioh, J. Lee, J. Han, S. Yoon, and G. Y. Ha, *J. Power Sources*, **140**, 59 (2005).
10. M. Ramani, B. S. Haran, R. E. White, and B. N. Popov, *J. Electrochem. Soc.*, **148**, A374 (2001).
11. B. E. Conway, *J. Electrochem. Soc.*, **138**, 1539 (1991).
12. A. Lobo and H. Conrad, *Surf. Sci.*, **523**, 279 (2003).
13. J. P. Zheng, P. J. Cygan, and T. R. Jow, *J. Electrochem. Soc.*, **142**, 2699 (1995).
14. B. E. Conway, *J. Electrochem. Soc.*, **138**, 1539 (1991).